Nanoscale

Accepted Manuscript

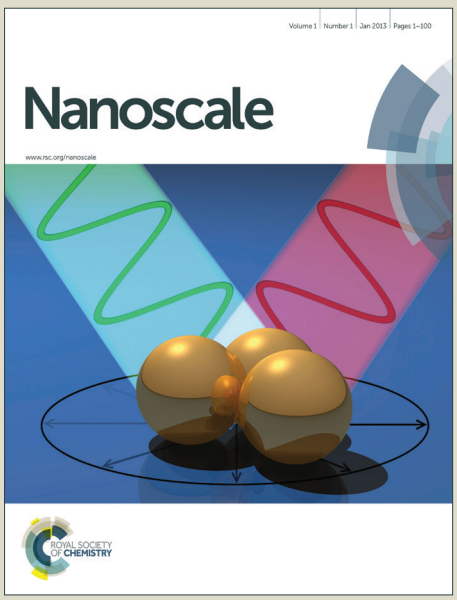

ROYAL SOCIETY OF CHEMISTRY

www.rsc.org/nanoscale

Molecular dynamics simulations of nanoscale and sub-nanoscale friction behavior between graphene and a silicon tip: Analysis of tip apex motion

Hong Min Yoon,[a] Youngmo Jung,[a] Seong Chan Jun,[a] Sasidhar Kondaraju,[b] and Joon Sang Lee[a,*]

[a]School of Mechanical Engineering, Yonsei University, 50 Yonsei-ro, Seoul, Korea 120-749

[b]Department of Mechanical Engineering, Indian Institute of Technology Delhi, Hauz Khas, New Delhi-110 016, India

*e-mail: joonlee@yonsei.ac.kr

Keywords: graphene multi-layers, molecular dynamics, friction between graphene layers, atomic force microscopy, lateral force microscopy, stick and slip behavior

ABSTRACT: A sliding object on a crystal surface with a nanoscale contact will always experience stick-slip movement. However, investigation of the slip motion itself is rarely performed due to the short slip duration. In this study, we performed molecular dynamics simulation and frictional force microscopy experiments for the precise observation of slip motion between a graphene layer and a crystalline silicon tip. The simulation results revealed a hierarchical structure of stick and slip motion. Nanoscale stick and slip motion is composed of sub-nanoscale stick and slip motion. Sub-nanoscale stick and slip motion occurred on a timescale of a few ps and a force scale of 10^{-1} nN. The relationship between the trajectories of the silicon tip and stick-slip peak revealed that in-plane and vertical motions of the tip provide information about stick and slip motion in the sub-nanoscale and nanoscale ranges, respectively. Parametric studies

including tip size, scan angle, layer thickness, and flexibility of the substrate were also carried out to compare the simulation results with lateral force microscopy findings.

1. Introduction

Graphene has attracted much attention in the field of tribology because of its unique crystal structure and mechanical properties.[1-5] Although graphene is very thin (approximately 0.38 nm), it has remarkable mechanical properties, especially in the in-plane direction. Graphene has a Young's modulus and breaking strength of 1 TPa and 130 GPa, respectively.[6] The atomic carbon bonding structure of graphene varies with directional orientation (*e.g.*, zigzag and armchair) according to the arrangement of carbon atoms because of the two-dimensional (2D) honeycomb lattice.

At the nanoscale, friction force microscopy (FFM) can be used to measure a lateral force as small as one-tenth of a nanonewton.[7] This resolution allows detailed investigation of a variety of parameters during frictional sliding, including the effects of crystal direction,[8, 9] normal load,[10] flexibility of substrate,[11] and contact area.[12,13] Many researchers have investigated the effect of these parameters on the behavior of stick-slip peaks since Mate *et al.* reported that the periodicity of a sample substrate induced a stick-slip movement of the tip when conducting FFM experiments.[14]

Dienwiebel *et al.* slid a graphite flake attached to a tungsten tip over a graphite substrate and observed high friction with a periodicity of 60° originating from the hexagonal-shaped graphene lattice.[9] Verhoeven *et al.* performed calculations using the Tomlinson model and provided a theoretical basis for the result of Dienwiebel *et al.*; they also calculated the potential energy of the surface and stick location.[8] Filippov *et al.* further demonstrated the existence of torque, which caused the graphene flake to stick when sliding on graphite.[15]

These studies indicate that the stick state is a local minimum energy state, the location of which is determined by the commensurability between two sliding surfaces.

Hence, stick-slip movement can be controlled by modifying the energy barrier magnitude near the stick state, which provides a smoother pathway for sliding. By doing so, the sliding object, *e.g.*, the tip in FFM, jumps from one stick state to the next. Maier *et al.* measured the slip time on the microscale and showed that slip time could be controlled by modifying the contact geometry.[16] Their results also showed an intermediate state during slow slip motion, implying that slip motion is a complex procedure rather than a simple jumping motion.

However, investigating the detailed mechanism of slip motion is difficult with current experimental techniques. Most slip events occur on a scale of nanometers and nanoseconds. In an FFM experiment, condition control is a complicated issue due to the various parameters that can affect the friction behavior, including surface roughness, temperature, defects, and oxidation. Hence, current experimental studies are limited to the measurement of average or maximum friction and describe only stick and slip patterns.

Molecular dynamics (MD) simulation is an effective way to provide supplemental information in an effort to mitigate the limitations of FFM experiments. Various interaction potentials have been developed to simulate materials including metals,[17,18] covalent materials,[19] and ionic compounds.[20,21] A recent review by Dong et al. described the approach of MD simulation on atomic-scale friction measurement.[22] The strength of MD simulation is that it can precisely mimic a phenomenon that occurs in a few fs or ps and provides a direct visualization of the friction phenomena. These characteristics help provide a detailed mechanism of friction phenomena at the nanoscale.[23-27]

Deng *et al.* used MD and finite element methods to show that strong elastic deformation and adhesion of graphene cause a negative friction coefficient.[23] Ye *et al.* also performed MD studies that showed the effect of the number and size of graphene layers on friction at the

nanoscale.[24] Moreover, they showed that the concept of flexural rigidity can only be applied for large, multi-layered graphene. Dong *et al.* constructed a hydrogenated graphene surface to study the hydrogenation effect that can easily occur under experimental conditions.[25] Hydrogenation enhances friction by increasing the atomic roughness.

In the present study, we performed MD simulations and FFM experiments to investigate stick and slip motion on the nanoscale and sub-nanoscale. Graphene layers were deposited on a SiO_2 substrate, and a crystalline Si tip was slid across the graphene surface. Scan angle and number of graphene layers were controlled to compare MD simulation results and FFM experiments. The comparisons validated our results and clearly showed the angular dependency and the effect of flexibility, which agreed well with previous studies. In MD simulations, friction data revealed sub-nanoscale stick-slip movements during nanoscale slip motion, demonstrating a hierarchical structure of stick-slip motion. We expanded these results to describe the relationship between the nanoscale and sub-nanoscale stick-slip motion and the motions of the tip apex.

2. Methods

Molecular dynamics simulations

The MD simulation mimicked the Si tip apex motion in the FFM experiment. Figure 1 (a) illustrates the overall simulation system, which consisted of four components: a crystalline SiO_2 substrate, a graphene layer, a crystalline Si tip apex, and a moving support. The graphene layer was located on a crystalline SiO_2 substrate and was 15 nm × 15 nm. As shown in Fig. 1 (a), the hemisphere tip apex was composed of 292 Si atoms with a radius of 1.2 nm. (In the tip size dependency, different sizes of tip were used). The tip was described as a rigid body and initially positioned at the lower left part of the graphene layer. The moving support, which is represented by blue atoms in Fig. 1 (b), had no atomic interaction with the other

atoms in the simulation system. The moving support had a constant velocity of 0.01 nm/ps. A harmonic spring was connected to the moving support and tip apex.

The simulation involved two steps. In the first step, a normal load was applied to the tip apex, which then began to interact with the graphene layer. A Lennard-Jones (LJ) potential was used to describe the Si-C interaction according to the LJ parameters provided by Ong and Pop.[28] C-C interaction in the graphene layer was modeled using the adaptive intermolecular reactive empirical bond order (AIREBO) potential.[29] The Tersoff potential was used for Si-Si and Si-O interactions in the SiO_2 substrate. The simulation was conducted for 1 ns to obtain an equilibrated system. We assumed that there was no oxidation and roughness effect during MD simulation.

The second step is illustrated in Fig. 1 (b). We applied a constant in-plane velocity on the moving support. Therefore, the support began to move in the scan direction with constant velocity, causing displacement between the support and tip apex. Three types of forces acted on the tip apex as follows: i) the interaction force between the tip apex and the graphene layer, $\vec{F}_{LJ}$, ii) the harmonic spring force, $\vec{F}_{spring}$, and iii) the external force (normal load), $\vec{F}_{load}$. The total force was the sum of these individual force components:

$$\vec{F} = \vec{F}_{LJ} + \vec{F}_{spring} + \vec{F}_{load} \quad (1)$$

The tip apex position was determined as the sum of the three force types. The friction force was defined as:

$$\vec{F}_{friction} = k(\vec{r}_{moving\ support} - \vec{r}_{tip\ apex}) \quad (2)$$

where k is the harmonic spring constant, and $\vec{r}_{moving\ support}$ and $\vec{r}_{tip\ apex}$ are the positions of the moving support and tip apex, respectively. An additional 1 ns of simulation was performed to obtain information on friction and tip apex position. The data were collected at a resolution of 0.1 ps. The canonical ensemble was used with a Langevin

thermostat at 10 K to minimize thermal effect. For all cases, 40 nN and 10 J/m^2 were used for load and spring constants, respectively. A large-scale atomic/molecular massively parallel simulator (LAMMPS) and Visual Molecular Dynamics (VMD) were used for calculations and post-processing, respectively.

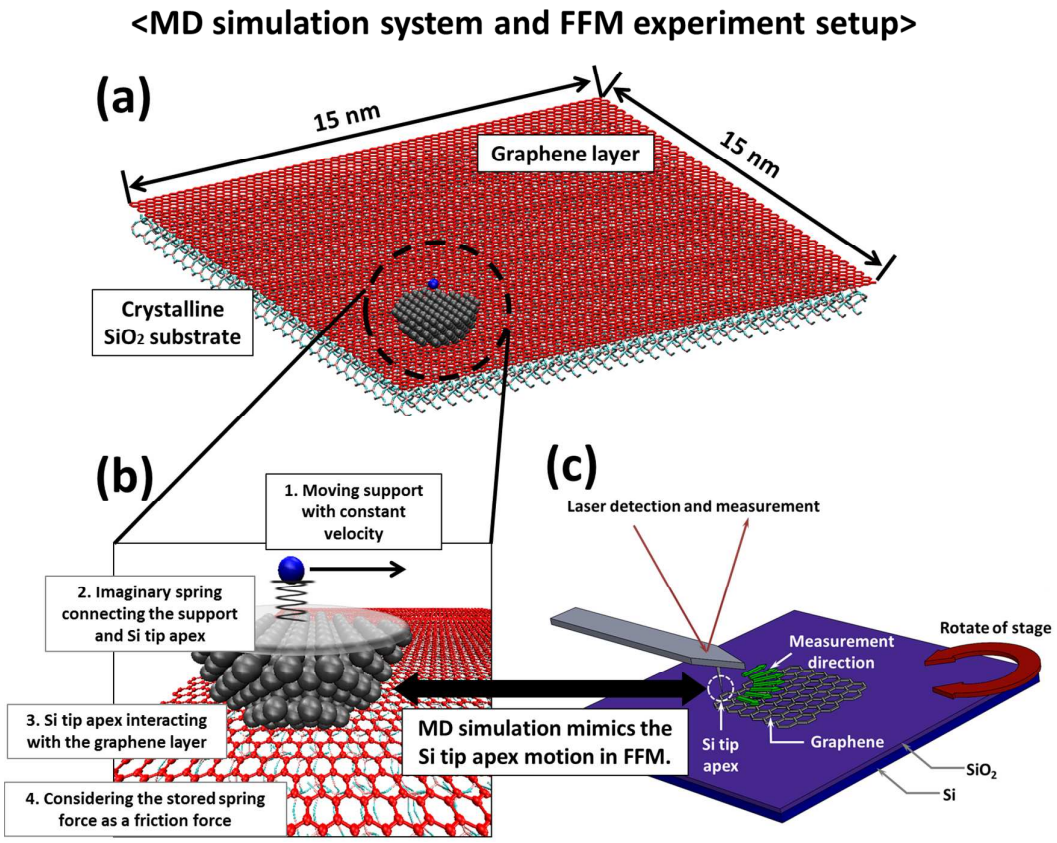

Figure 1. Schematic of (a) the MD simulation system, (b) the detailed simulation process, and (c) the FFM experiment setup.

Friction force microscopy (FFM) experiments

Mono-, bi-, and tri-layer graphene films were prepared on a Si/SiO_2 wafer using mechanical exfoliation from highly oriented pyrolytic graphite (HOPG) under atmospheric pressure to produce intrinsic graphene terraces. The measured graphene layer was identified using an optical microscope. The local layer thickness of the films was identified via Raman spectroscopy by analyzing the D and G peaks of the Raman spectra.

In Fig. 1 (c), the experimental set-up of FFM is described. Frictional properties of each graphene sample were measured in a sealed box at room temperature using an atomic force microscope (AFM, XE 100, Park Scientific Instruments, South Korea). We used the crystalline Si tip with a radius of 16 nm (NCS36, Mikromasch). To achieve high-resolution lateral force imaging, we used a silicon contact mode tip on a cantilever; its thickness and length were 1 μm and 130 μm, respectively. Contact mode was employed with a feedback scheme to control vertical bending. The normal force of the contact tip was 20 nN, and the contact and release signal behaviors of the tip were analyzed using normal force for determining tip sensitivity.

Topographic and lateral force images were taken simultaneously at a 1 Hz scan speed over a 5 nm × 5 nm area. First, we determined the atomic direction of graphene using topology and lateral force microscope images. After the first measurement, the scan angle was varied from 0° (zigzag direction) to 90° (armchair direction) in mono-, bi-, and tri-layer graphene by rotation of the measurement stage.

3. Results and discussion

Figure 2 describes the structure of the results and discussion sections. Main objective of this study is to find the hierarchical structure of stick and slip behavior, and its relation with the tip apex motion. In the first section, we controlled the scan angle and flexibility of the simulation system, and compared the MD simulation and FFM experiments results to validate the simulation model. In the following section includes the motivation of this study. In this section we varied the size of tip, and showed the existence of sub-nanoscale stick and slip motions during nanoscale stick and slip motion. Then, the results of two different scan angles, armchair and zigzag, from the previous validation section were chosen for the detail analysis of the sub-nanoscale stick and slip behavior and its correlation with the in-plane tip apex

motion. In the last section, relation of the nanoscale stick and slip motion and the vertical motion of tip apex was also developed using the results of flexibility effect.

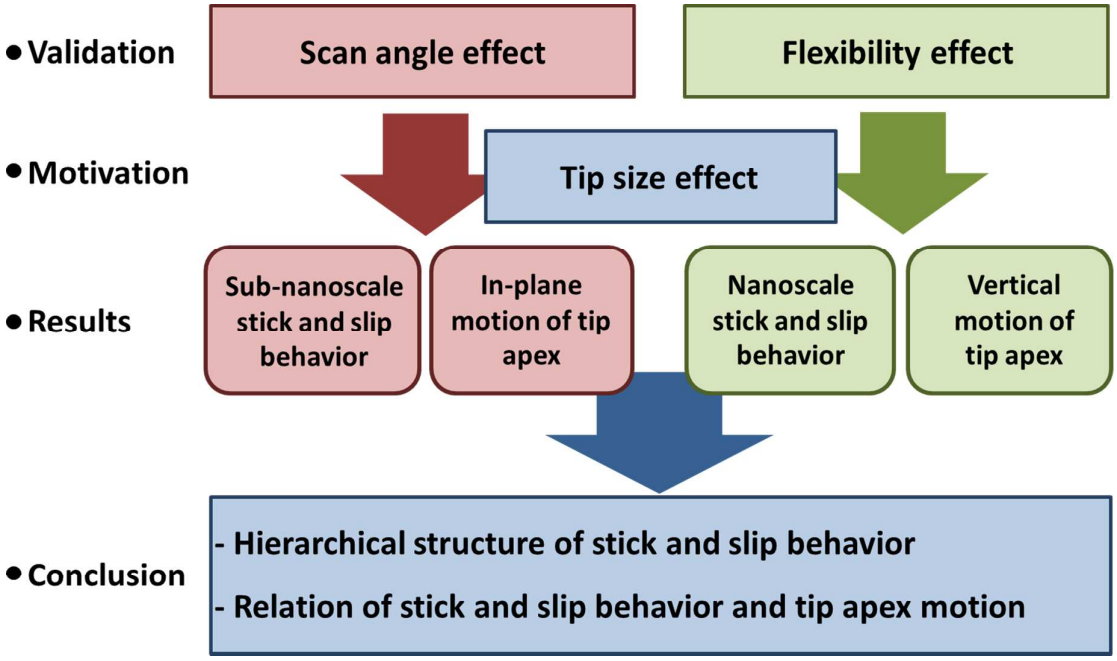

Figure 2. Schematic diagram of the structure of the results and discussions section.

Validation: scan angle and flexibility effect

In order to determine the relationship between graphene atomic structure and applied frictional force, we measured the frictional force for mono-layer graphene using AFM in FFM mode. Graphene samples extracted by mechanical exfoliation were prepared (four samples for each layer) and were measured repeatedly at a normal force of 20 nN. Using the same method, we measured each sample at varied orientations of 0° to 180° (Fig. 3 (c)).

The atomic structure of graphene is presented in Fig. 3 (a), as measured by AFM. Figure 3 (b) shows an enlarged area of the red box in Fig. 3 (a). In this area, graphene has a zigzag structure when the scan direction is 0º and has an armchair structure when the scan direction is 90º (inset of Fig. 3 (b)).

Figure 3 (c) shows the schematic of simulations performed to determine the scan angle

dependency of friction. As shown in Fig. 3 (c), the tip apex was initially located at the lower left corner of the graphene. The zigzag direction was set as the scan angle of 0°. We increased the scan angle by units of 15° up to 90° (armchair direction). Rigid graphene and SiO_2 substrate were used to study the effect of scan angle by excluding the puckering effect.

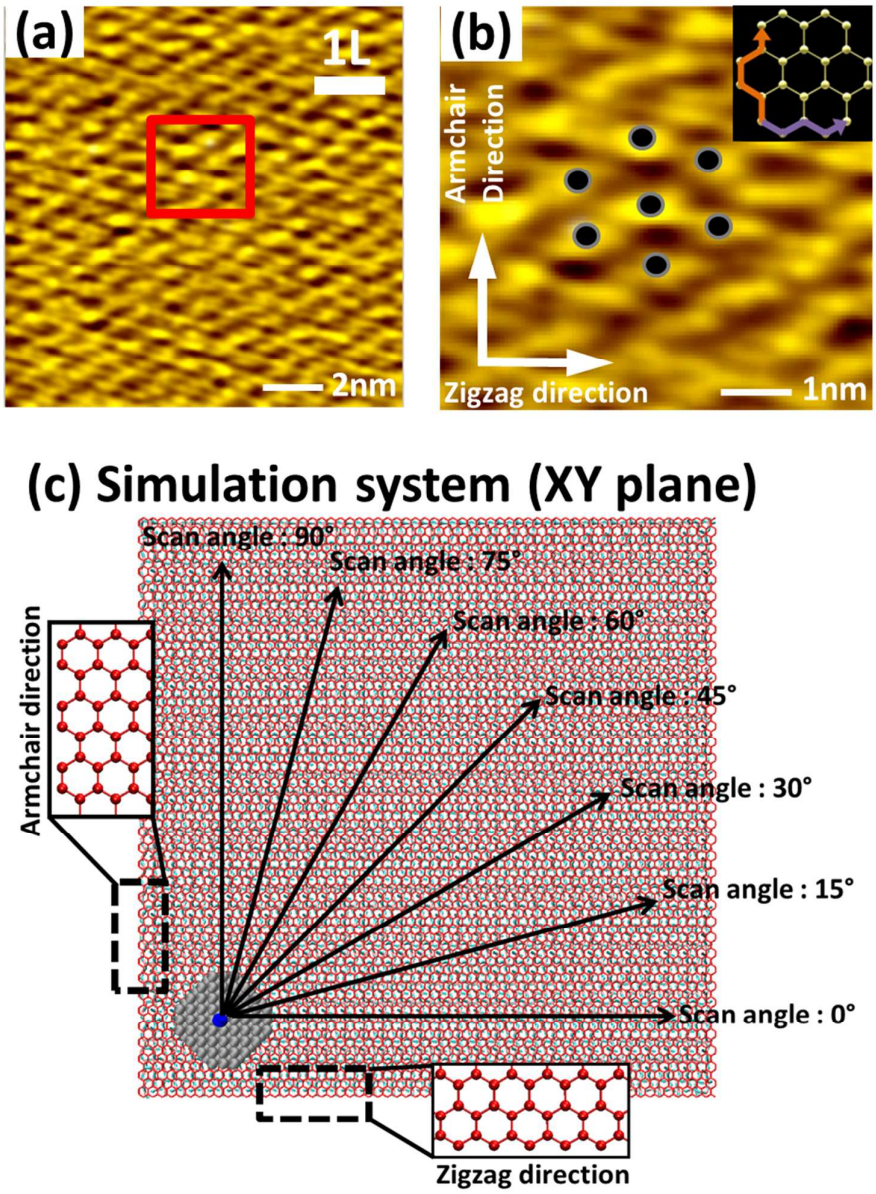

Figure 3. Atomic structure of graphene measured by AFM in a 5 nm× 5 nm area (a) in mono-layer graphene, (b) expanded area in red box, and schematic diagram of scan direction and atomic structure of graphene (inset). (c) Schematic of the simulation system for studying scan angle dependency.

Figure 4 shows the scan angle dependency of the average friction. The black filled circles and blue empty squares represent the FFM and MD results, respectively. Two different Y-axes are used to show the similar trends in scan angle dependency. In FFM experiments, the friction was measured 35 times in each direction. There was no significant change in friction value from the average (Fig. S1). The friction results show the lowest values at 0° and 60° (zigzag direction) and the highest values at 30° and 90° (armchair direction). This was due to the honeycomb lattice of graphene, which has a periodicity of 60°. A previous FFM experiment and theoretical calculation also showed the friction properties with a periodicity of 60° for a graphite system.[8, 9]

As shown in Fig. 4, the magnitude of friction in FFM was larger than that in MD. In nanoscale, friction is proportional to contact area, with contact area being the main factor determining friction magnitude. During MD simulation, the radius of the tip was 1.2 nm compared to the 16 nm in the FFM experiment. The size of the tip was much larger in simulations and could have induced the larger contact area in the FFM experiment compared to that in the MD simulation. Furthermore, the puckering effect was excluded from the simulation through the use of a rigid graphene layer. This condition created a relatively small contact area between the tip apex and the graphene layer in MD simulations. On the other hand, in the experiments, the contact area between the tip apex and graphene layer was increased by the puckering effect. The large contact area induced a strong adhesion force and friction force.[30] However, the variation in friction in FFM was less than that in MD. The puckered surface caused a strain in the graphene layer and deformed the graphene morphology. The deformed graphene surface became an imperfect crystal, resulting in the decreased the effect of scan angle .[31]

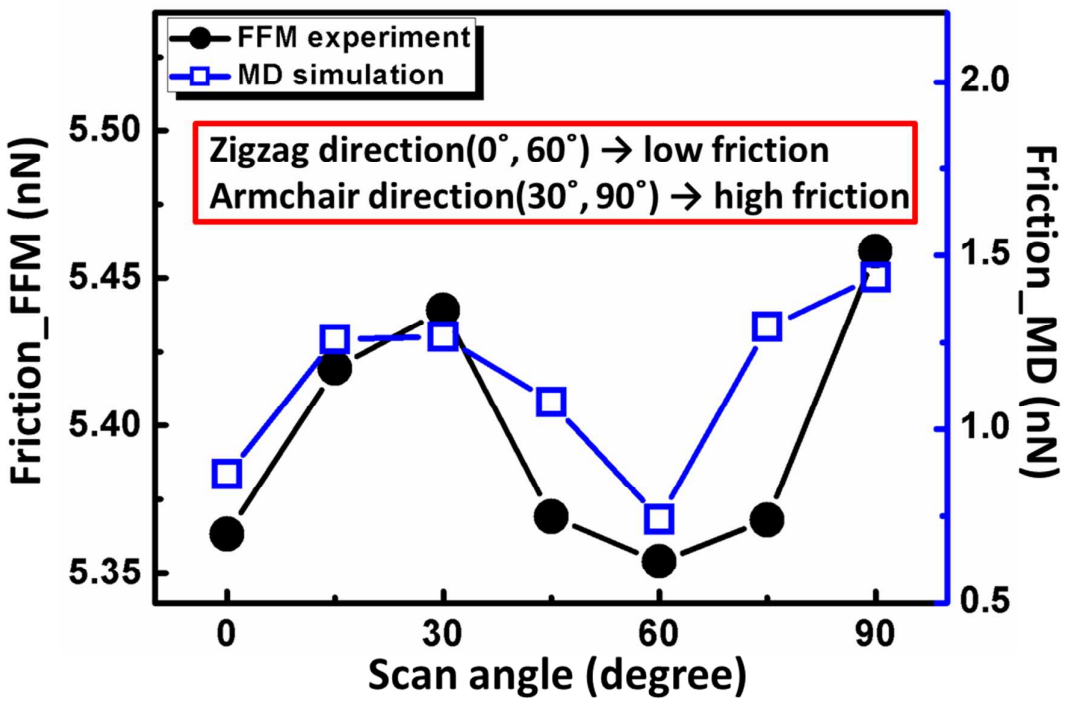

Figure 4. The scan angle dependency of friction in FFM experiments and MD simulations.

Topological properties of graphene samples were analyzed by AFM measurement. Figures 5 (a), (b), and (c) show topographic images of mono-, bi-, and tri-layered graphene, respectively. The height of the mono-layer graphene is 0.34 nm and is proportional to the number of layers. Vertical height difference was measured by AFM, as shown in Fig. 5 (d). The standard line of each graphene was normalized at 0, and the vertical height difference was measured to be 0.39 nm in mono-layer, 0.77 nm in bi-layer, 1.23 nm in tri-layer graphene. Figure 5 (e) shows the Raman spectra evolution at 633 nm as a function of the number of layers.

Each spectrum provides the known fingerprint features associated with graphene. The intensity of the spectrum for mono-layer graphene was lower than that of the other layered graphene. For all samples, first-order Raman allowed observation of the G band (~1582 cm^{-1}) and the strong G' band (~2600 cm^{-1}). The G peak at 1583 cm^{-1} corresponds to graphene zone-center phonons, and it is the only band originating from a normal first-order Raman scattering

process in graphene. On the other hand, the G' originates from a second-order process involving two ITO phonons near the K point for the G' band. The G' peak is at 2626 cm^{-1} for the mono-layer, at 2647 cm^{-1} for the bi-layer, and is at 2663 cm^{-1} for the tri-layer graphene. For all samples, the G peak is around 1582 cm^{-1}, and the G' band intensity is greater than that of the G band. The absence of a D peak in the samples indicates that the sample is largely defect-free.

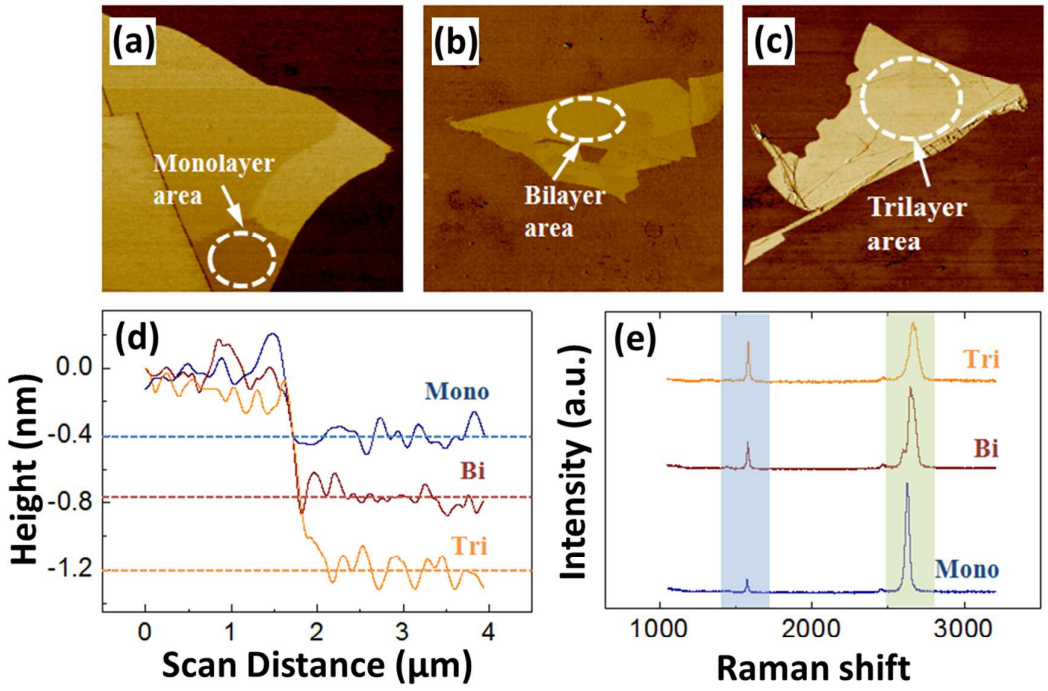

Figure 5. Images of graphene samples obtained by mechanical exfoliation from graphite: (a) mono-layer, (b) bi-layer, (c) tri-layer graphene. (d) 633 nm Raman spectra, (e) the height of each graphene layer.

Three simulations were performed to illustrate the effect of graphene flexibility and the SiO_2 substrate. As shown in Figs. 6 (a), (b), and (c), Type 1, Type 2, and Type 3 represent rigid graphene with a rigid SiO_2 substrate, flexible graphene with a rigid SiO_2 substrate, and flexible graphene with a flexible SiO_2 substrate, respectively. In Fig. 6 (b), only the graphene layer is puckered. In Fig. 6 (c), the SiO_2 substrate is also puckered together with the shape of the tip apex.

The number of graphene layers was varied up to four to clarify the effect of flexibility of the

graphene and substrate at a scan angle of 30°. In Fig. 6, the results of three simulation types are compared with the experiment results. Black squares, red circles, blue up-triangles, and green down-triangles represent the results of Type 1, Type 2, Type 3, and FFM experiments, respectively. A previous study has demonstrated that the puckering effect decreased as the number of graphene layers increased. Friction also decreased as the puckering effect decreased as a result of the change in contact area.[11] All results noted in Fig. 6 clearly show the decreasing trend in friction with increase in graphene layers.

In Type 1 simulations, the variation in friction is relatively small compared to that in Type 2 and Type 3 because of the rigid graphene layer that hindered the puckering of graphene. In Type 2 and 3 simulations, the system had flexibility which induced large contact area, and caused the strong adhesion between the tip apex and graphene layer.

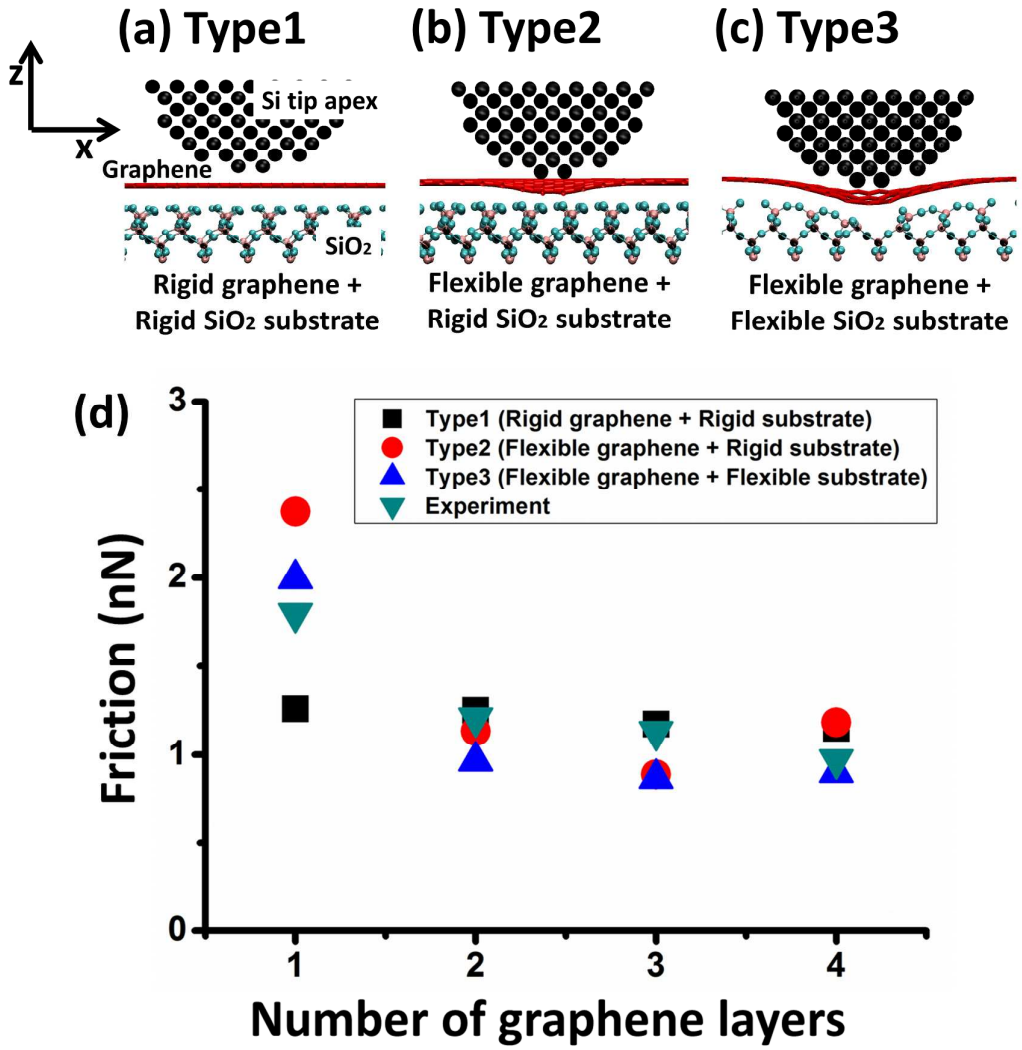

Figure 6. Three different types of simulation snapshots describing the flexibility of graphene and SiO2 substrates. (a) Type 1: Flexible graphene with rigid SiO2 substrate. (b) Type 2: Rigid graphene with rigid SiO2 substrate. (c) Type 3: Flexible graphene with flexible SiO2 substrate. (d) Dependency of friction on flexibility of the graphene and SiO2 substrate. The graphene layer thickness varied from mono-layer to quad-layer. Black squares, red circles, blue up-triangles, and green down-triangles represent the results of Type 1, Type 2, and Type 3 simulations, and experiments, respectively.

Motivation: effect of tip size on slip behavior

We varied the radius of the tip to analyze the effect of tip size on slip motion. The scan angle was set to 0° (zigzag direction) for all cases. Figures 7 (a), (b), and (c) represent the structure of the tip with radii of 0.6, 0.9, and 1.2 nm, respectively.

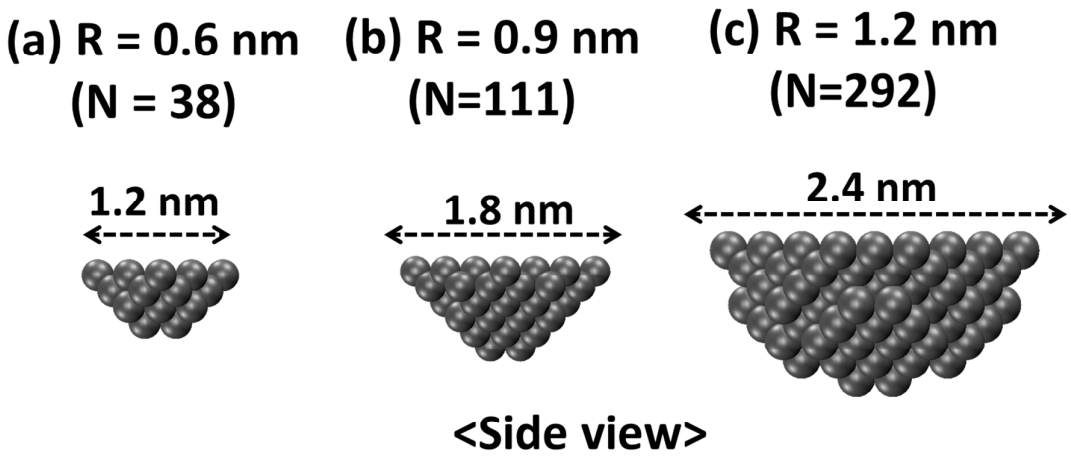

Figure 7. Structure of the crystalline silicon tip with the radii of (a) 0.6 nm, (b) 0.9 nm, and (c) 1.2 nm.

Figure 8 (a) shows the stick-slip movement of the initial 300 ps. Regular and stable stick-slip movements were observed for all cases. Black filled arrows indicate the maximum friction where the slip motion started. Maximum friction increases as the radius of the tip increases due to the increase in contact area between the Si tip and graphene mono-layer. We have defined the contact area based on the cutoff distance of interaction between graphene and silicon tip. By this definition, the contact area was measured up to the first and second nearest atoms in silicon tip. The numbers of atoms in a contact area were 13 and 25 for the case of the tip radius of 0.6 and 1.2 nm, respectively (Fig. S2). The three tips show different stick and slip patterns. In the simulation, differences in contact area induced a different contact geometry and energy state for the different tip sizes. We performed energy calculation with the initial contact state of two different tip radii. The case with the radius of 0.6 nm has two strong interaction points with the magnitude of interaction energy in the order of 10^6. On the other hand, the case with the radius of 1.2 nm has four strong interaction points with the magnitude of interaction energy in the order of 10^2 (Fig. S3).

We selected a simulation period between 125 ps and 175 ps for all cases and then normalized the friction values using the maximum friction indicated by the black filled arrow. In Fig. 8

(b), the X and Y axes represent the time and normalized friction, respectively. Measured slip duration values were 3.9, 7.7, and 18.8 ps for tip radii of 0.6, 0.9, and 1.2 nm, respectively. The small tip showed short slip duration, while the larger tip showed relatively long slip duration. In Fig. 8 (b), the black empty arrows clearly show the existence of an intermediate state during slip motion. The increase in slip duration was caused by the change in contact geometry between graphene and the Si tip. These results agreed with Maier et al.'s finding regarding the effect of contact geometry on slip duration.[16]

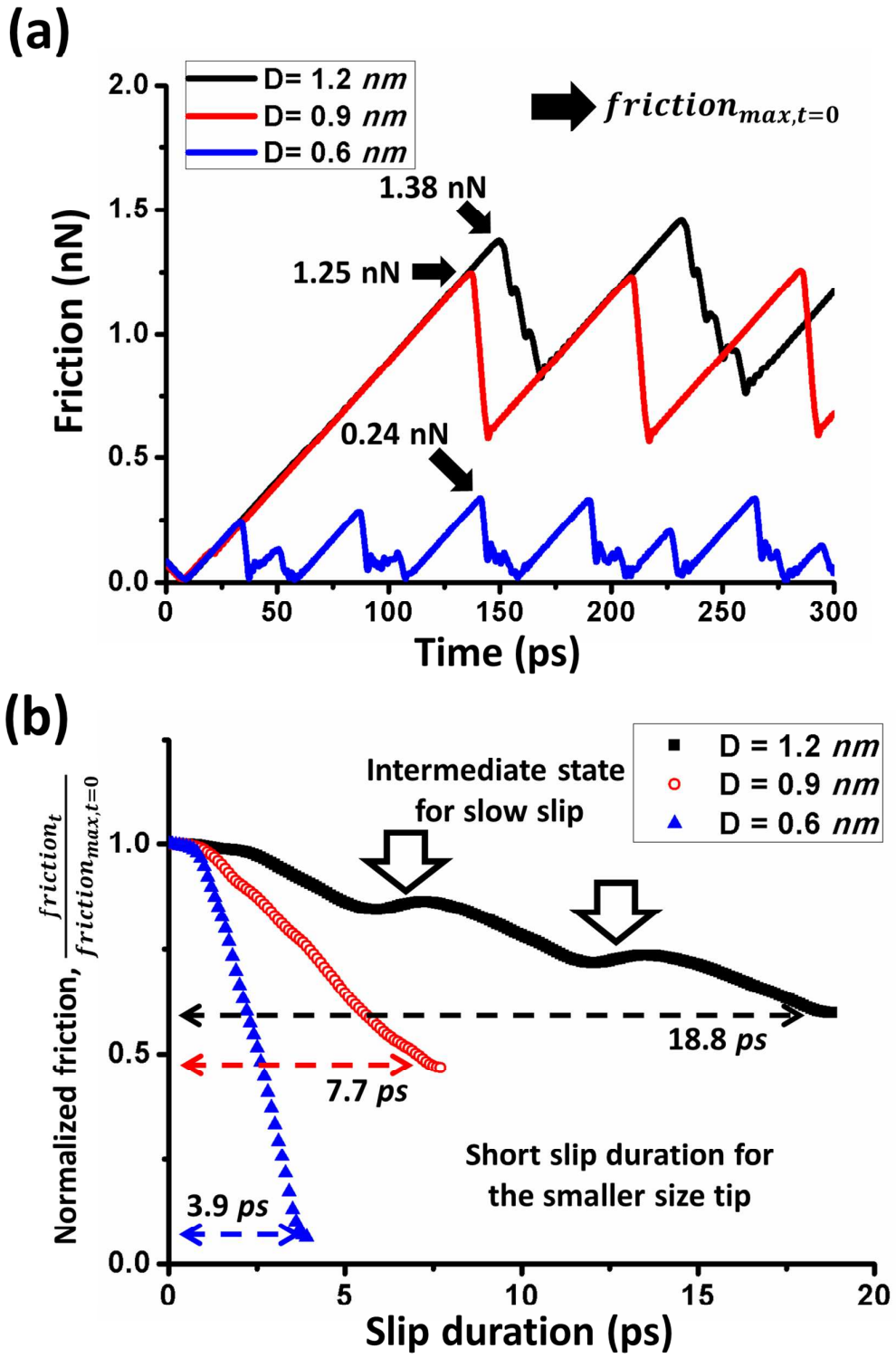

Figure 8. (a) Stick-slip movement with three different tip radii of 0.6, 0.9, and 1.2 nm. Black filled arrows indicate the maximum friction and starting point of the selected slip motion for each case. (b) Variation in normalized friction during the selected slip motion. Black empty arrows clearly show the intermediate states in slip motion.

Sub-nanoscale stick and slip behavior

Figure 9 shows the time dependence of friction in the zigzag direction (scan angle: 0°) and armchair direction (scan angle: 90°). Maximum friction values observed for zigzag and armchair directions were 1.38 nN and 2.40 nN, respectively. Both plots show nanoscale stick and slip behavior. Stick motion occurred when the tip apex was located at an energetically stable position. Hence, maximum friction can represent the energy required to move to the next stick position. In Figs. 9 (a) and (b), a larger number of peaks and smaller magnitude of maximum friction were observed in the zigzag direction compared to those in the armchair direction, implying that the silicon tip changed its stick position with less energy in the zigzag direction (Fig. S4).

Insets in Figs. 9 (a) and (b) provide enlarged plots of the friction results during slip motion. During the nanoscale slip motion, sub-nanoscale stick and slip motion exists, as indicated by the black filled arrow in the insets of Figs. 9 (a) and (b). These sub-nanoscale stick and slip motions occurred continuously during nanoscale slip motion. The distance between two nearest neighboring points represents the variation in friction during 0.1 ps. The slip duration in nanoscale and sub-nanoscale were about 20 ps and 3 ps, respectively.

We calculated the center of mass position for the tip apex in the XY plane to assess the relationship between friction and motion of the tip apex. Figures 9 (c) and (d) show the trajectory of the tip apex for the zigzag and armchair directions during the time periods of 509 ~ 620 ps and 655 ~ 814 ps, respectively. Both plots clearly represent regular motion of the tip apex. The motion of the tip apex in the XY plane contains information about sub-nanoscale stick and slip motion. The density of the data set can be used to analyze sub-nanoscale stick and slip motion. The black filled arrows in Figs. 9 (c) and (d) indicate sub-nanoscale stick and slip motion. As shown, the tip apex moved slowly in the region with the dense data set, and then fast motion was observed when slip occurred, which is represented

by the sparse data set. The shape of the trajectory is similar to the arrangement of graphene atoms. Zigzag- and armchair-shaped trajectories of the tip apex are shown in Figs. 9 (c) and (d), respectively.

The density of data set could be quantized as a velocity of the tip apex. Figures 9 (e) and (f) show the variation in the tip apex velocities of the zigzag and armchair direction, respectively. We calculated scan direction velocity for the both cases. Black filled arrows indicate the nanoscale stick and slip motion. Scan direction velocities maintained zero when the nanoscale stick motion occurred. On the other hand, the velocities were subsequently increased when the nanoscale slip motion occurred. And then, the velocity fluctuated until the end of the slip motion. Inset of Figs. 9 (e) and (f) expand this fluctuation which shows the sub-nanoscale stick and slip motion.

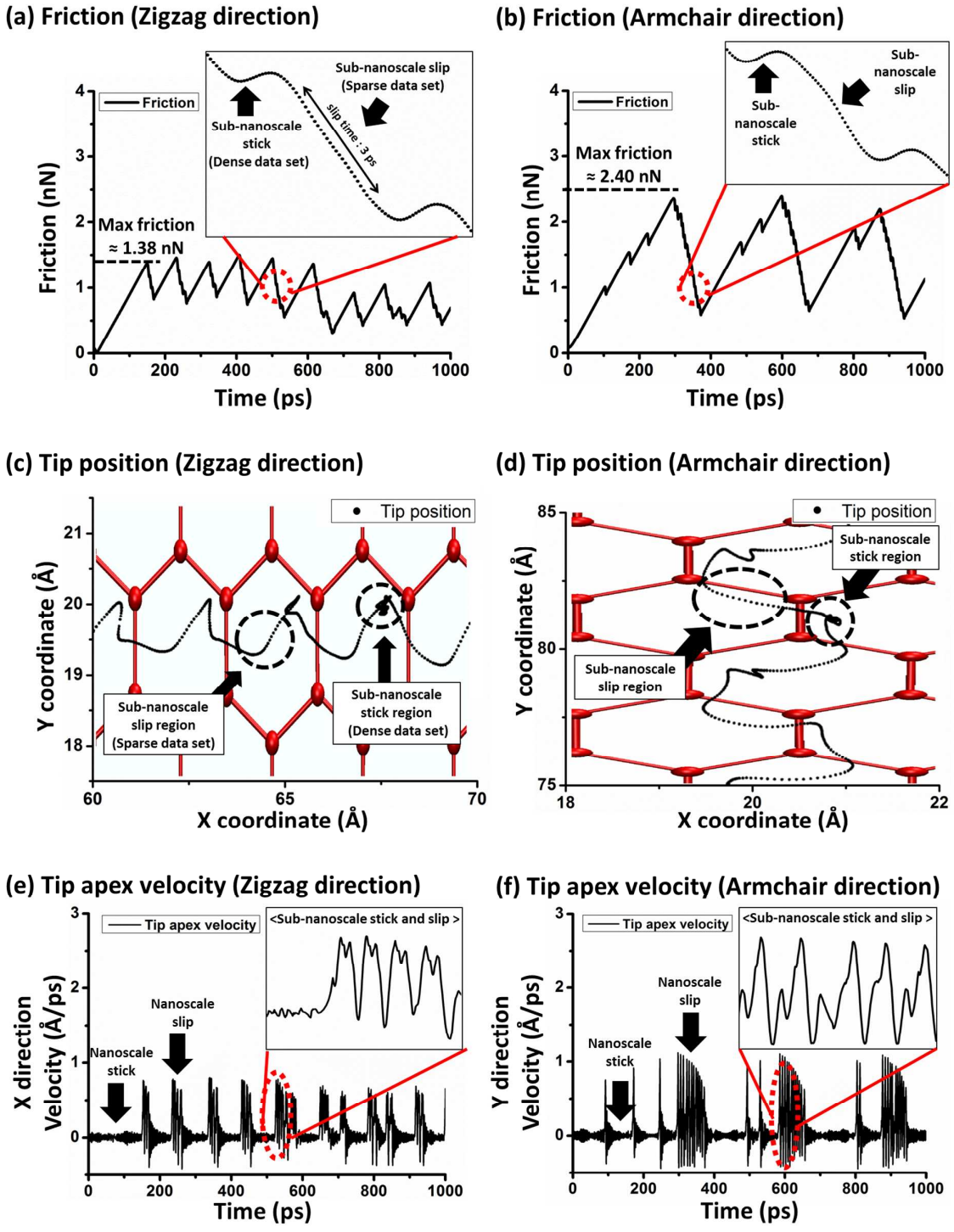

Figure 9. Friction vs. time in the (a) zigzag direction and (b) armchair direction. The insets of each graph show the existence of sub-scale stick and slip motion. Trajectory of the tip apex center of mass in the (c) zigzag direction and (d) armchair direction in the XY plane. Each graph shows regular movement of the tip apex. Dense and sparse data sets represent stick and slip events, respectively. Friction and tip position data clearly show the occurrence of sub-nanoscale stick and slip motion. The scan direction velocity of (e) zigzag direction and (f) armchair direction.

Relationship between nanoscale slip behavior and the vertical motion of the tip apex

In Fig. 10, black and blue lines show the time series of friction and tip apex height for the mono-layer cases of Type 1, Type 2, and Type 3, respectively. These three types of simulations clearly show the nanoscale stick and slip behavior. The blue lines represent the tip apex height, defined as the vertical position of the mass center. The average height of the tip apex was the highest in Type 1 and the lowest in Type 3. As shown in Fig. 10 (b), friction showed a stable stick and slip peak for Type 1, wherein the tip apex maintained its vertical position better than for Type 2 and Type 3. This is due to the rigid graphene and SiO_2 substrate, which prevent the puckering effect. On the other hand, relatively active vertical motion is observed in Fig. 10 (c) for Type 3. The magnitudes of change in height of the tip apexes were about 0.1, 0.2, and 0.5 Å for Type 1, Type 2, and Type 3, respectively. The flexible graphene and SiO_2 substrate affected the vertical motion.

In Fig. 10 (a), red arrows indicate the one-to-one correspondence between the nanoscale slip motion and the large vertical motion of the tip apex. We also calculated the vertical velocity of the tip apex. The magnitude of fluctuation of the velocity also increased when nanoscale slip motion occurred (Fig. S5). A slip event is known to be an energy release process in a friction system.[32] Hence, the one-to-one correspondence of nanoscale slip motion and large vertical motion of tip apex implies that the tip apex releases energy by vertical motion. The same trends were also observed in Type 2 and Type 3, although the magnitudes of the vertical tip apex motion were different. In the previous section, information regarding the in-plane motion of the tip apex only explained the sub-nanoscale stick and slip motion, while the vertical motion of the tip apex determined the nanoscale stick and slip motion. We observed the same trend with varying graphene thickness. In those cases, as the number of layers was increased, the vertical motion-driven slip was suppressed (Fig. S6).

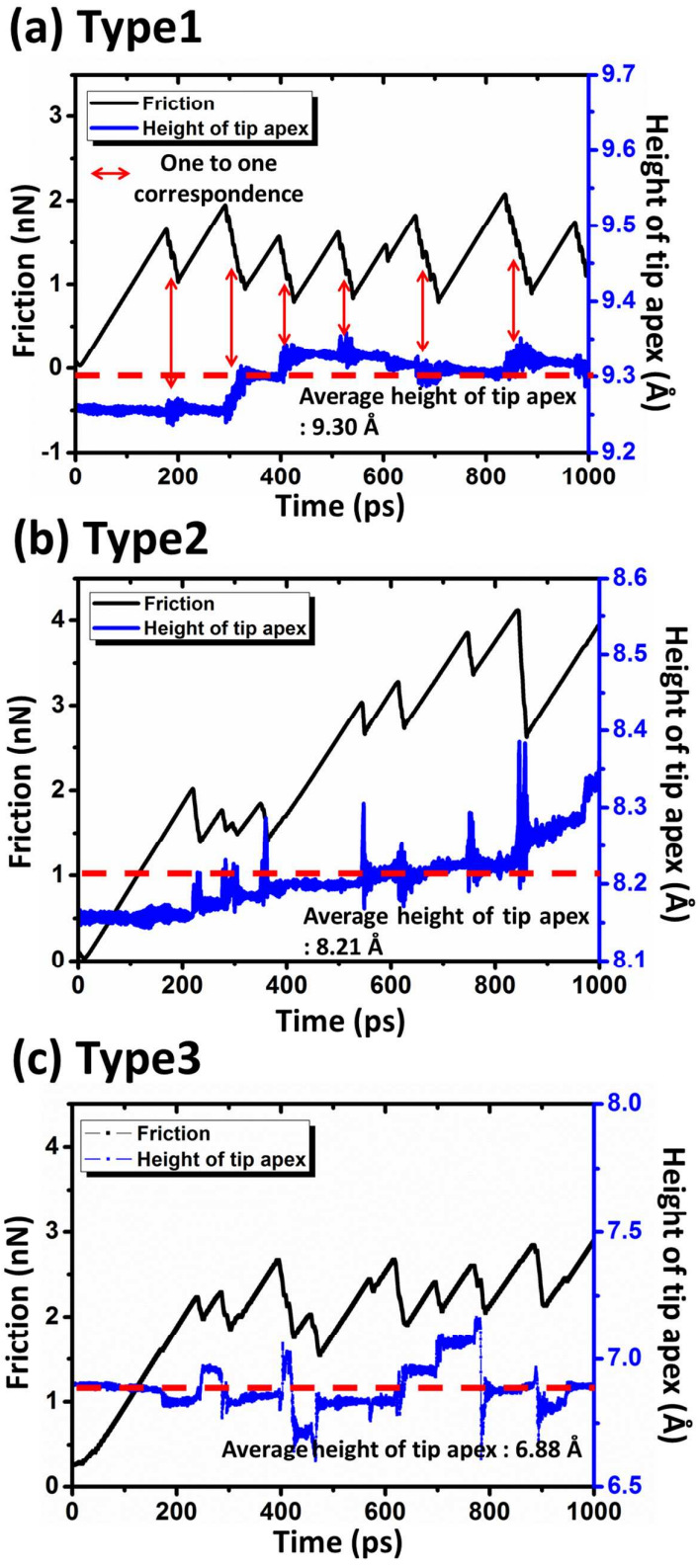

Figure 10. Time series of the friction and tip apex height for (a) Type 1, (b) Type 2, and (c) Type 3. Left and right sides of the Y-axis represent friction and tip apex height, respectively.

4. Conclusions

In this study, we simulated the motion of a Si tip apex on a graphene layer. Our simulation results showed clear nanoscale and sub-nanoscale stick and slip behavior. The dependencies on scan angle and flexibility were consistent with the results of the FFM experiment. Friction in the armchair direction was higher than that in the zigzag direction. In the time series of the friction plot, sub-nanoscale stick and slip motion was continuously observed during nanoscale stick and slip motion. Trajectories and velocity of the tip apex also provided sub-nanoscale stick and slip information. Regular in-plane motion was continuously repeated, and the shape of the trajectory is similar to the arrangement of graphene atoms. We found the strong relation of the sub-nanoscale stick and slip behavior and the in-plane motion of the tip apex. The flexibility of graphene and the SiO_2 substrate significantly affected the nanoscale stick and slip behavior and the vertical motion of tip apex. The magnitude of the vertical motion was the lowest in the case of the rigid graphene with a rigid SiO_2 substrate. We showed that vertical motion of the tip apex had a one-to-one correspondence with the nanoscale slip motion. This implies that vertical motion of the tip apex is an important parameter in determining nanoscale slip motion.

In present study, we excluded the effects of the roughness caused by substrate and thermal fluctuation, and oxidation to clearly observe sub-nanoscale friction behavior. These effects should be included when considering the realistic situation.

Acknowledgements

This work was supported by a Grant from the Mid-career Researcher Program of the National

Research Foundation of Korea (NRF) funded by the Ministry of Science, ICT and Future Planning (Grant No. NRF-2013R1A2A2A01015333).

References

1. C. G. Lee, X. D. Wei, J. W. Kysar and J. Hone, *Science*, 2008, **321**, 385-388.

2. C. Gómez-Navarro, M. Burghard and K. Kern. *Nano Lett*., 2008, **8**, 2045-2049.

3. D. H. Cho, L. Wang, J. S. Kim, G. H. Lee, E. S. Kim, S. H. Lee, S. Y. Lee, J. Hone and C. G. Lee, *Nanoscale*, 2013, **5**, 3063-3069.

4. Z. Xu, X. Li, B. I. Yakobsonc and F. Ding. *Nanoscale*, 2013, **5**, 6736-6741.

5. X. Zhang, B. R. S. Rajaraman, H. Liub and S. Ramakrishna, *RSC Adv*., 2014, **4**, 28987-29011.

6. A. K. Geim, *Science*, 2009, **324**, 1530-1534.

7. H. J. Kim and D. E. Kim, *Int. J. Perecis. Eng. Manuf.*, 2009, **10**, 141-151.

8. G. S. Verhoeven, M. Dienwiebel and J. W. M. Frenken, *Phys. Rev. B*, 2004, **70**, 165418.

9. M. Dienwiebel, N. Pradeep, G. S. Verhoeven, H. W. Zandbergen and J. W. M. Frenken, *Surf. Sci*., 2005, **576**, 197–211.

10. T. Filleter, J. L. McChesney, A. Bostwick, E. Rotenberg, K. V. Emtsev, Th. Seyller, K. Horn, and R. Bennewitz, *Phys. Rev. Lett.*, 2009, **102**, 086102.

11. C. G. Lee, Q. Li, W. Kalb, X. Z. Liu, H. Berger, R. W. Carpick and J. Hone, *Science*, 2010, **328**, 76-80.

12. R. W. Carpick, D. F. Ogletree and M. Salmeron, *J. Colloid Interface Sci.*, 1999, **211**, 395-400.

13. M. A. Lantz, S. J. O'Shea and M. E. Welland, *Phys. Rev. B*, 1997, **55**, 10776-10785.

14. C. M. Mate, G. M. McClelland, R. Erlandsson and S. Chiang, *Phys. Rev. Lett*., 1987, **59**, 1942 -1987.

15. A. E. Filippov, M. Dienwiebel, J. W. M. Frenken, J. Klafter and M. Urbakh, *Phys. Rev. Lett.*, 2008, **100**, 046102.

16. Maier, Y. Sang, T. Filleter, M. Grant and R. Bennewitz, *Phys. Rev. B*, 2005, **72**, 245418.

17. M. S. Daw and M. I. Baskes, Phys. Rev. B 1984, 29, 6443.

18.M. I. Baskes, J. S. Nelson, and A. F. Wright, Phys. Rev. B 1989, 40, 6085.

19. D. W. Brenner, Phys. Rev. B 1990, 42, 9458.

20 S. Maier, E. Gnecco, A. Baratoff, R. Bennewitz, and E. Meyer, Phys.Rev. B 2008, 78, 045432.

21. S. Maier, Y. Sang, T. Filleter, M. Grant, R. Bennewitz, E. Gnecco, and E. Meyer, Phys. Rev. B 2005, 72, 245418.

22. Y. Dong, Q. Li, and A. Martini, *J. Vac. Sci. Technol.*, A, 2013, **31**, 030801.

23. Z. Deng, A. Smolyanitsky, Q. Li, X. Q. Feng and R. J. Cannara, *Nat. Mater.*, 2012, **11**, 1032–1037.

24. Z. Ye, C. Tang, Y. Dong and A. Martini, *J. Appl. Phys.*, 2012, **112**, 116102.

25. Y. Dong, X. Wu and A. Martini, *Nanotechnology*, 2013, **24**, 375701.

26. H. M. Yoon, S. Kondaraju and J. S. Lee, *Tribol. Int.*, 2014, **70**, 170-178.

27. H. J. Kim and D. E. Kim, *Nanoscale*, 2012, **4**, 3937-3944.

28. Z. Y. Ong and E. Pop, *Phys. Rev. B*, 2010, **81**, 155408.

29. S. J. Stuart, A. B. Tutein, and J. A. Harrison, *J. Chem. Phys.*, 2000, **112**, 6472-6486.

30. Q. Li, C. Lee, R. W. Crpick, and J. Hone, *Phys. Status Solidi B*, 2010, **247**, 2909-2914.

31. A. V. Khomenko and N. V. Prodanov, *Carbon*, 2010, **48**, 1234-1243.

32. M. Dienwiebel, G. S. Verhoeven, N. Pradeep, J. W. M. Frenken, J. A. Heimberg and H. W. Zandbergen, *Phys. Rev. Lett.*, 2004, **92**, 126101.